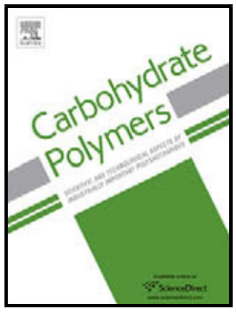

Title: Continuous flow adsorption of ciprofloxacin by using a nanostructured chitin/graphene oxide hybrid material

Authors: Joaquín Antonio González, Jonathan Germán Bafico, María Emilia Villanueva, Sergio Alejandro Giorgieri, Guillermo Javier Copello

PII: S0144-8617(18)30159-0
DOI: https://doi.org/10.1016/j.carbpol.2018.02.021
Reference: CARP 13283

To appear in:

Received date: 29-11-2017
Revised date: 5-2-2018
Accepted date: 6-2-2018

Please cite this article as: González, Joaquín Antonio., Bafico, Jonathan Germán., Villanueva, María Emilia., Giorgieri, Sergio Alejandro., & Copello, Guillermo Javier., Continuous flow adsorption of ciprofloxacin by using a nanostructured chitin/graphene oxide hybrid material.*Carbohydrate Polymers* https://doi.org/10.1016/j.carbpol.2018.02.021

Continuous flow adsorption of ciprofloxacin by using a nanostructured chitin/graphene oxide hybrid material

Joaquín Antonio González[a,b], Jonathan Germán Bafico[a], María Emilia Villanueva[a,b], Sergio Alejandro Giorgieri[a], Guillermo Javier Copello[a,b,*]

[a]*Universidad de Buenos Aires (UBA), Facultad de Farmacia y Bioquímica, Departamento de Química Analítica y Fisicoquímica, (UBA), Junín 956, C1113AAD Buenos Aires, Argentina*
[b]*Instituto de Química y Metabolismo del Fármaco, Facultad de Farmacia y Bioquímica, (IQUIMEFA-UBA-CONICET), Argentina*
**Corresponding author: Química Analítica Instrumental, FFyB, UBA, Junín 956 - Piso 3 (C1113AAD), CABA, Argentina. Tel.: +54 11 49648254; fax: +54 11 49648254. E-mail:* gcopello@ffyb.uba.ar

Graphical abstract

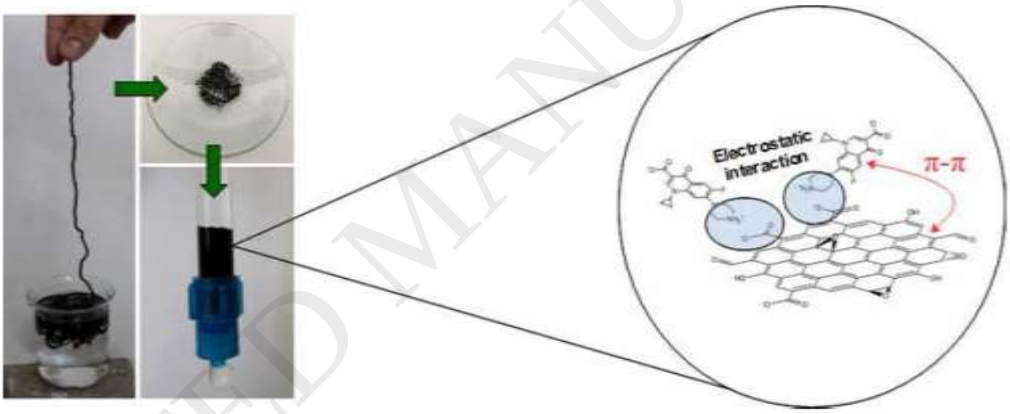

Highlights

- Chitin:nGO hybrid is used as ciprofloxacin continuous adsorbent for the first time.
- Components' source and matrix reusability make this material a low-cost adsorbent.
- The material adsorption performance is strongly dependent of medium pH.
- The chitin:nGO probes to be applicable to real water samples.

Abstract

A novel nanostructured material was successfully developed by combining a chitin matrix with graphene oxide nanosheets (Chi:nGO) and then used for the continuous flow adsorption of ciprofloxacin. The spectroscopic characterization indicated that none covalent interaction between both components would be occurring and the introduction of nGO did not interfere in chitin nanostructure

rearrangement during gelling and later drying. SEM images and Mercury Intrusion Porosimetry results showed a wide pore size distribution ranging from nano to micrometers. The continuous flow adsorption was observed to be dependent on the pH which affects the electrostatic interaction. The flow rate, Na^+ concentration and water hardness were evaluated to describe the adsorption process. The resistance to alkali allowed to regenerate and reuse the column for subsequent adsorption cycles. Finally, ciprofloxacin spiked real water samples were assessed and the results confirmed that the medium pH was the main parameter that defines the adsorption behavior.

Keywords: chitin; graphene oxide nanosheets; nanocomposite; continuous adsorption.

Introduction

Emerging contaminants are defined as chemicals that had not been previously detected in water supplies (or were found in far lesser concentrations) and nowadays are discovered either in surface water or groundwater (Petrie, Barden, & Kasprzyk-Hordern, 2015; Van Doorslaer, Dewulf, Van Langenhove, & Demeestere, 2014). The main groups of emerging contaminants are pharmaceuticals, personal care products and endocrine disrupting compounds which could persist in the environment including the drinking water since the purification processes are not designed to eliminate them (Matamoros, Rodríguez, & Albaigés, 2016). Among the pharmaceutical products, ciprofloxacin is a synthetic antimicrobial derived from nalidixic acid and is one the most common fluoroquinolone used for antibiotic therapies in humans for urinary and respiratory infections. Moreover, the use of ciprofloxacin in veterinary has been raising the last years since it is applied not only as therapeutic but also with prophylactic purposes in cattle, poultry and shrimp farming (Holmström et al., 2003; Teuber, 2001). The main sources of contamination are hospital wastewater and feedlots, being excretions of humans and animals disposed almost intact due to its low metabolism. The contact with the environment represents a threat taking into account that it would induce the proliferation of bacterial resistance (Sharma, Johnson, Cizmas, McDonald, & Kim, 2016). Ciprofloxacin has been determined

in water and wastewater at concentrations ranging from < 1 µg/L up to 6.5 mg/L in some cases (Fick et al., 2009).

In the last years several research works described different methods for ciprofloxacin decontamination. Some of those techniques are enzymatic degradation, electrochemical and chemical oxidation, photocatalysis and adsorption (Chen, Gao, & Li, 2015; Ji, Ferronato, Salvador, Yang, & Chovelon, 2014; Prieto, Möder, Rodil, Adrian, & Marco-Urrea, 2011; Y. Wang, Shen, Zhang, Zhang, & Yu, 2016; Yan et al., 2013). Most of them present high implementation costs or are not capable to achieve good water quality except for adsorption which has a good performance against different contaminants, for example organic molecules like antibiotics (Rodriguez-Narvaez, Peralta-Hernandez, Goonetilleke, & Bandala, 2017). One of the advantages of adsorption is the opportunity of scale up; also, during the treatment, no co-products are released to the environment. Moreover, either in batch or continuous process, after saturation is reached, many of the adsorbent materials can be recovered and reused (Huang, Fulton, & Keller, 2016).

Currently carbon and its allotropes, such as graphene, carbon nanotubes and fullerene have acquired an important role in the development of new nanostructured materials with several applications in the water remediation field (Ma et al., 2016; Ncibi & Sillanpää, 2015; Rodriguez-Narvaez et al., 2017; Suárez-Iglesias, Collado, Oulego, & Díaz, 2017). Graphene is a one-atom thick layer of graphite where the carbon atoms are distributed in a regular sp^2-bonded network and is one of the most studied materials for the research of new materials with uncountable applications including pollutant adsorbents due to its extremely high specific surface (2630 m^2/g) (Bonaccorso et al., 2015; Novoselov, 2004). However, its low solubility, reactivity and high production cost represent a drawback when it comes to using it at high scale for the adsorption of polar molecules. The synthesis of graphene oxide nanosheets (nGO) is a facile and low-cost method for increasing the hydrophilicity and reactivity of the nanomaterial because of the addition of oxidized functional groups through the chemical exfoliation of graphite (Sharif, Gagnon, Mulmi, & Roberts, 2017).

Chitin, an abundant biopolymer present in nature, can be found in fungi, the exoskeleton of insects and the shells of crustaceans, including shrimp and crab, as well as other invertebrates, such as marine sponges (Guo, Duan, Zhou, & Zhu,

2014). Its structure consists predominantly of unbranched chains of β-(1→4)-2-acetoamido-2-deoxy-d-glucose. The main source of chitin are the disposals of food industry, making it a low-cost and sustainable material for polymeric matrices synthesis since has a good stability against different liquid media, for instance organic solvents and acid or basic conditions (Guo, Duan, Cui, & Zhu, 2015). Considering its use in column adsorption processes, the porous-like structure of this polysaccharide exhibits a good performance against increasing flows and allows to work at low pressure (Ma et al., 2016; McKay, Blair, & Gardner, 1984).

We state the hypothesis that a nanostructured hybrid material composed by chitin loaded with nGO can be synthetized by means of a simple method and successfully applied in a continuous flow system for the adsorption of ciprofloxacin as an emerging contaminant model. Therefore, the aim of the present work is to test the dynamic adsorption behavior of the hybrid and study the main parameters that affect its performance, including real water samples. Although several researchers have already proved the capability of adsorption of ciprofloxacin by using pure nGO or combined in different polymeric matrices most of them only describe the behavior of the material in batch systems. Furthermore, up to our knowledge, there is not any background in literature regarding the implementation of nGO in continuous column systems against emerging contaminants.

2. Materials and methods

2.1. Reagents and materials

Chitin from shrimp shells was obtained from Sigma-Aldrich (USA, calculated degree of acetylation, DA: 95 %). Graphite fine powder extra pure (particle size < 50 μm) was acquired from Merck (Germany). Calcium chloride dihydrate was purchased from Cicarelli (Argentina); Methanol was acquired from Sintorgan (Argentina). Ciprofloxacin hydrochloride was purchased from Saporiti (Argentina). Water was filtered and deionized with a Milli-Q, Millipore system (Milford, MA, USA). All other reagents were of analytical grade.

Tap-water was collected from Buenos Aires Autonomous City (Argentina) and well-water samples were collected from Chascomús city (Buenos Aires province, Argentina) and Macachín city (La Pampa province, Argentina). Tap-water samples

were collected from household taps connected to the city water supply network. Well-water samples were collected from household taps connected to systems of water pumped from wells. Before collecting the samples, water was let run for 5 min. Waters were stored at 4 °C until the assays.

2.2. Preparation of the Chi:nGO hybrid matrix

The nGO was prepared through Hummers method as described elsewhere (Hummers Jr & Offeman, 1958). The resulting graphite oxide was exfoliated into graphene oxide monolayer nanosheets (nGO) by sonication at 35 kHz for 30 min after dispersion in citrate buffer (0.4 M; pH 4.20). Then the suspension was centrifuged, and the pellet was washed with water and then with methanol. The methanol was removed by heating in a stove at 60 °C and the graphene oxide powder was then stored at room temperature.

The chitin suspension was prepared according to Tamura *et al* (Tamura, Nagahama, & Tokura, 2006). Briefly, 42.5 g of calcium chloride dihydrate were suspended in 50 mL of methanol and refluxed for 30 min at 82 °C to a state of near-dissolution. One gram of chitin powder was poured into the calcium solvent and refluxed for 2 h at 90 °C with stirring.

In order to obtain a hybrid material with a chitin:graphene oxide (Chi:nGO) ratio of 3:1, 10 g of chitin suspension, containing 120 mg of pure chitin, was mixed with 40 mg of nGO. The Chi:nGO 3:1 proportion was chosen based on our previous work, where it was observed that lower proportions of nGO presented lower adsorption capacities and higher nGO proportions do not increment significantly the adsorption capacity (González, Villanueva, Piehl, & Copello, 2015). Wet-spinning method was applied for gelling the Chi:nGO mixture which was loaded into a syringe and then injected in methanol cooled between -10 and -8 °C. The gel strand was washed several times with methanol and ultra-pure water to wash out all the methanol and $CaCl_2$ residues. Finally, the gel strand was dried in stove at 60 °C until constant weight, grinded and sieved by using a 35-mesh filter. In order to study the effect of nGO addition, the same procedure mentioned above was applied for the obtaining of a chitin particle material (Chi).

2.3. Chi:nGO matrix characterization

FTIR and FT-Raman spectra were recorded using a Nicolet iS50 Advanced Spectrometer (Thermo Scientific). FTIR spectra of nGO, Chi and Chi:nGO were recorded with 32 scans and a resolution of 4 cm^{-1} whereas FT-Raman spectra of pristine chitin powder and Chi were acquired with an excitation laser beam of 1064 nm, 0.25 W laser power, resolution of 4 cm^{-1}, 150 scans. All samples were previously dried for 24 h at 60 ºC to avoid water related bands interference. Chitin degree of acetylation (DA) was determined by the method proposed by Brugnerotto *et al.*, which is based on the relationship between a reference band at 1420 cm^{-1} and the amide III band at 1320 cm^{-1} by applying the following equation: A1320/A1420 = 0.3822 + 0.03133DA (Brugnerotto et al., 2001).

The investigation of the ultrastructure of Chi and Chi:nGO was performed by Small Angle X-ray Scattering using the SAXS1 beamline of the National Synchrotron Light Laboratory (LNLS), Campinas, Brazil. The SAXS measurements were performed at room temperature in transmission geometry with λ = 1.55 Å (8 keV). The 2D SAXS spectra were monitored using a Pilatus 300K detector. A sample to-detector distance of 0.9 and 3 m and an exposure time of 60 s were used. The samples were placed with their surfaces perpendicular to the direction of the incident X-ray beam and parallel to the X-ray detector. The scattering intensity (I) was measured as a function of the scattering vector (q) from 0.004 to 0.26 $Å^{-1}$. The background and parasitic scattering were determined by using an empty sample holder and were subtracted for each measurement. Scattering profiles modeling was performed using SASfit software (Breßler, Kohlbrecher, & Thünemann, 2015).

Scanning Electron Microscopy (SEM) images of freeze-dried and gold coated samples were taken using a Pillips 505 microscope. Mercury intrusion porosity (MIP) tests were performed by using a Porosimeter 2000 Carlo Erba and pressures ranging from 1 to 2000 kg/cm^2. The intrusion volumes were measured at stepwise increasing pressures equilibrating at each pressure step.

The pH of the point of zero charge (pH_{pzc}) of Chi:nGO 3:1 was determined by the drift method, where the pH point at which the curve of the final pH crosses the $pH_{initial} = pH_{final}$ line is the pH_{pzc} (Lopez-Ramon, Stoeckli, Moreno-Castilla, & Carrasco-Marin, 1999).

2.4. Adsorption experiments

2.4.1. Batch experiment

Isotherm experiment was carried out by a batch method at room temperature (25 °C) with constant stirring (120 rpm). 10 mg of Chi:nGO powder were put in contact with 2 mL of ciprofloxacin solutions in ultra-pure water (pH 6.30) ranging from 4 to 850 mg/L. Absorbance determinations were carried out at the characteristic absorption peak by using an UV–Vis Spectrophotometer (Cecil CE 3021, Cambridge, England). The equilibrium adsorption capacity, q_e (mg/g), for all experiments was determined by a mass balance on the ciprofloxacin,

$$q_e = \frac{(C_0 - C_e) \times V}{m} \quad (1)$$

where C_0 (mg/L) is the initial concentration, C_e (mg/L) is the equilibrium concentration in the liquid phase, V (L) is the volume of liquid phase, and m (g) is the mass of the adsorbent.

Blank experiments were conducted to verify the absence of sorbate precipitation and/or adsorption to the walls of the microtubes.

2.4.2 Column adsorption assays and regeneration

In order to describe the behavior of the matrix against a water source polluted with ciprofloxacin, a series of experiments were conducted analyzing: flow rate, pH of ciprofloxacin solution, sodium and calcium concentration and real water samples from different sources spiked with ciprofloxacin. One hundred grams of Chi:nGO 3:1 were packed into a Sigma Liquid Chromatography Lauer Lock glass column (1.0 cm inner diameter and 10 cm in height) with a 1.5 cm bed height. The matrix was preconditioned by washing it with several volumes of ultra-pure water, 0.1 M HCl, ultra-pure water, 0.1 NaOH and ultra-pure water again, in that order. Ciprofloxacin solutions were pumped by High Precision Pump P-500 (Pharmacia) and the effluent concentration was determined by UV detection at 280 nm by using an online FPLC detector (Pharmacia). All data were collected and analyzed through PC-Chrom software. Upon column exhaustion, the adsorbed antibiotic was eluted by using 0.1 M NaOH followed by ultra-pure water until absorbance reached baseline. The breakthrough curves were plotted as C_t/C_0 vs time (min),

$$\frac{C_t}{C_0} = \frac{Effluent\ concentration\ at\ time\ t\ (\frac{mg}{L})}{Influent\ concentration\ (\frac{mg}{L})} \quad (2)$$

2.4.3. Mathematical analysis

The behavior of the adsorbent for all the tested conditions was mathematically analyzed and described applying a nonlinear regression to Thomas and Yoon-Nelson breakthrough curve models.

The Thomas model assumes Langmuir kinetics of adsorption-desorption and no axial dispersion is derived with the assumption that the rate driving force obeys second-order reversible reaction kinetics. The model was used to calculate the maximum solid phase concentration of ciprofloxacin on adsorbent and the adsorption rate constant. The expression of the kinetic model is given below (Han et al., 2009),

$$\frac{C_t}{C_0} = \frac{1}{e^{(\frac{k_{Th}}{Q}\times(q_0\times m)-(C_o\times Q\times t)}} \quad (3)$$

where, C_0 and C_t are respectively the influent and effluent concentrations (mg/mL), k_{Th} is the Thomas rate constant (mL/mg min), q_0 is maximum dynamic adsorption capacity (mg/g), t is time (min), m is the mass of adsorbent in the column (g) and Q is the flow rate (mL/min).

The Yoon–Nelson model assumes that the rate of decrease in the probability of adsorption for each adsorbate molecule is proportional to the probability of adsorbate adsorption and the probability of adsorbate breakthrough on the adsorbent. It does not require further information about characteristics of adsorbate, the type of adsorbent, and the physical properties of the adsorption bed. The expression of the kinetic model is given below (Han et al., 2009),

$$\frac{C_t}{C_0} = \frac{e^{(k_{YN}\times t-k_{YN}\times\tau)}}{1+e^{(k_{YN}\times t-k_{YN}\times\tau)}} \quad (4)$$

where, k_{YN} is the rate constant (min^{-1}), τ is time required for 50 % adsorbate breakthrough (min) and t is time (min).

2.5. Characterization of real water samples

The pH of all samples was measured by pHmeter. Natural water cation composition studies were carried out by capillary electrophoresis by using a Capel 105M with UV-Vis detector (Lumex, Russia). The capillary column used was 40 cm length and 50 μm inner diameter; constant temperature of 25 °C; injection at 10 mBar for 5 s; constant voltage of 25 kV and indirect detection at 214 nm. The background electrolyte composition was buffer acetic acid/sodium acetate pH 4.40, 15 mM creatinine and 15 mM hydroxyisobutyric acid (HIBA).

2.6. Goodness-of-fit analysis

All experiments and their corresponding measurements were conducted in triplicate under identical conditions and the goodness-of-fit was evaluated by the root mean square error (RMSE) (Hadi, Samarghandi, & McKay, 2010).

3. Results and discussion

3.1. Characterization of the nGO and Chi:nGO 3:1 matrix

3.1.1. Spectroscopic characterization

Fig. 1 shows all the spectra of the raw materials, the intermediate components and the final Chi:nGO 3:1 hybrid. In comparison with the graphite FTIR signals, the graphene oxide spectrum shows an increase in the bands corresponding to oxidized groups, which confirms the chemical exfoliation of graphite into. The slight band at 1240 cm^{-1} is attributed to the C–O–C bond stretching which demonstrates the formation of epoxy groups. Moreover, the presence of carboxyl and carbonyl functional groups can also be detected at 1400 and 1730 cm^{-1}, which corresponds to C–OH and C=O stretching, respectively (Li, Liu, & Ma, 2011). In the case of pristine chitin, its spectrum shows a doublet at 1655 and 1625 cm^{-1} corresponding to the amide I (C–O and C–N stretching, respectively). Other characteristic bands are the amide II band (1540 cm^{-1}, N–H stretching), that is detectable together with the amide III band (1390 cm^{-1}), and the glycosidic bond band at 900–1100 cm^{-1} (C–O–C stretching) (Saito, Putaux, Okano, Gaill, & Chanzy, 1997). After gelling from chitin to Chi, the doublet around 1640 cm^{-1} appears unified in only one signal and the glycosidic bond band slightly changes at 1010 cm^{-1} suggesting that during the chitin suspension and following gelling a new arrangement is taking place and the typical structure of α-chitin of crustaceans partially disappears. The Raman spectra of Chi and chitin powder,

showed in SD1, supports this results since the amide I signal at 1650 cm^{-1} turned into a broader signal instead of a clear doublet. Considering that this signal corresponds to the carbonyl amide group which is involved in the formation of hydrogen bondings, the difference between chitin powder and Chi spectra confirms the rearrangement among the chitin chains due to the gelling process (Focher, Naggi, Torri, Cosani, & Terbojevich, 1992). Finally, in the spectrum of Chi:nGO 3:1 one cannot observe any new bands or the disappearance of preexisting from the individual spectra of Chi or nGO which indicates that the interaction between chitin and nGO probably does not involve the formation of a new functional group as it was described before by González *et al.* (Gonzalez, Mazzobre, Villanueva, Diaz, & Copello, 2014).

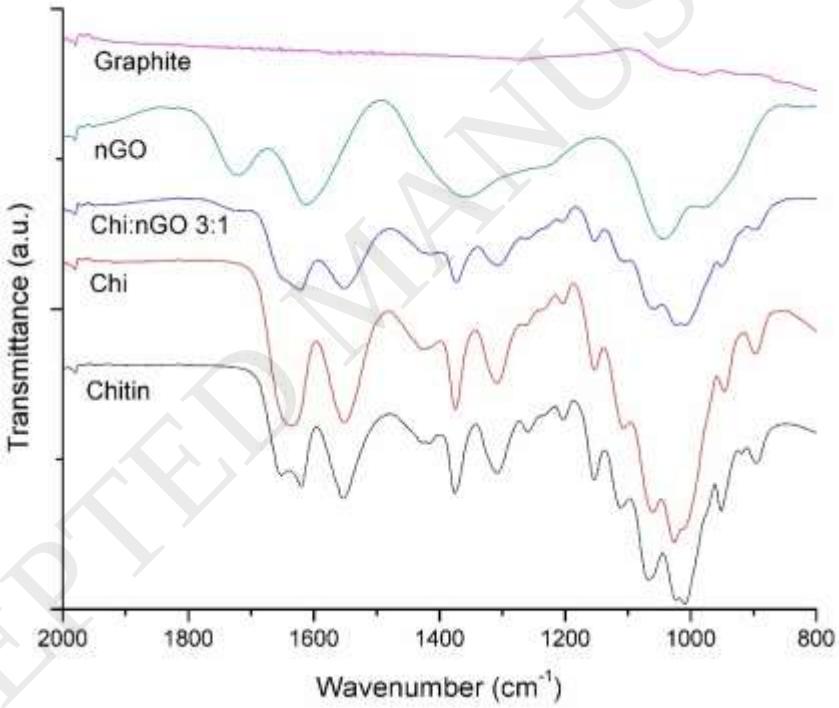

Fig. 1. FTIR spectra of graphite, nGO, Chi:nGO 3:1 hybrid, Chi and commercial chitin powder.

The nanostructure of the hydrogels obtained by the wet-spinning method and in the dried state were evaluated by means of the SAXS technique. Fig. 2 shows the SAXS profiles of commercial chitin powder, the Chi gels and Chi:nGO 3:1 hybrid at the wet and dried state, with subtraction of nGO profile according to the case. As can be observed, all profiles of the dried materials follow a power-law

behavior in the *q* range of ~0.004–0.04 Å^{-1}. For the wet materials, a distinct behavior is observed with a low slope regime followed by a higher slope section between 0.011-0.1 Å^{-1}, above which a short knee-like regime appears; the wet materials profiles are typical of disordered materials with more than one structural level. In the high slope section, all profiles were fitted according to the relation $I(q) \sim q^{-\alpha}$, where the exponent α is associated with the fractal characteristic of the material and with the network density (Beaucage, 1996; Brinker et al., 1984; Choudhary & Bhatia, 2012). In the case of dried material, the α values found were near 3 which is indicative of surface fractals and dense materials and, as could be expected, the wet materials present lower α around 2.3, indicative of mass fractals and more expanded networks.

In order to determine the local dimension at low *q* regime (lower slope) and the knee-like regime, the scattering profiles of the wet materials were modeled with the Beaucage unified equation for fractal materials with multiple structural levels (McConville, Whittaker, & Pope, 2002; Zhang et al., 2015),

$$I(q) \approx G^{\left(\frac{-q^2 R_g^2}{3}\right)} + B^{\left(\frac{-q^2 R_{sub}^2}{3}\right)} \left(\frac{1}{q^*}\right)^p + G_s^{\left(\frac{-q^2 R_s^2}{3}\right)} + B_s \left(\frac{1}{q_s^*}\right)^{P_s} \quad (5)$$

where G and G_s are the Guinier prefactors for the larger and smaller structures respectively, R_g is the radius of gyration, R_s is the smallest R_g observed at high *q*, whereas R_{sub} is at the high *q* limit, B and B_s are prefactors specific to the Power-law scattering, which are specified as the decay exponent P and P_s respectively, $q^* = q/[\mathrm{erf}\,(q\, k\, R_g/6^{1/2})]^3$ and $q_s^* = q/[\mathrm{erf}\,(q\, k_s\, R_s/6^{1/2})]^3$. As can be seen in Fig. 2, as well as the overall profile, the local dimensions of each regime for both Chi gels and the Chi:nGO 3:1 hybrid appears at similar *q*. This would mean that the introduction of the nGO is not altering the conformation of the polysaccharide. The modeling with Beaucage unified equation confirms this result based on the similar parameter values obtained: for the knee-like regime at high *q*, the R_{sub} value represented a small ordering of the chitin chains at 14.60 ± 0.07 nm and 13.88 ± 0.07 nm for Chi gel and Chi:nGO 3:1, respectively. On the other hand, at lower *q*, larger structures are represented by the R_g with values of 131.2 ± 0.2 nm and 149.4 ± 0.2 nm, respectively. As it was mentioned above, after drying, these structures collapse leading to more packed materials.

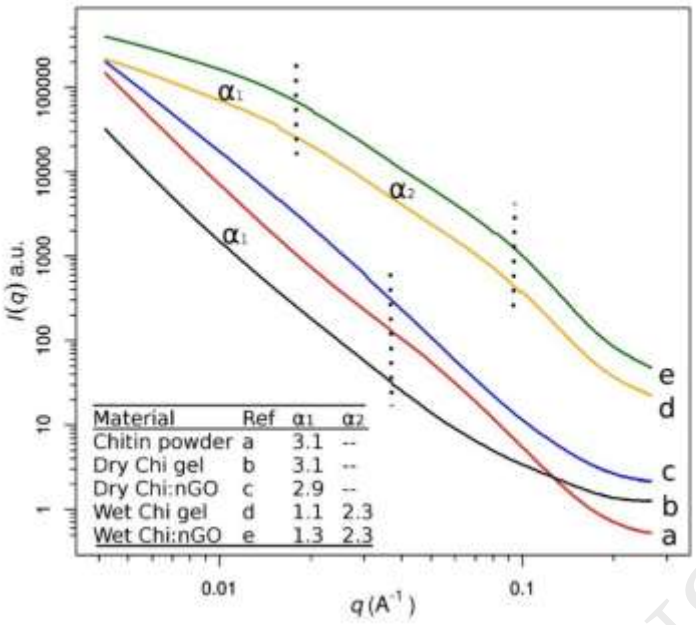

Fig. 2. SAXS profiles of commercial chitin powder and Chi and Chi:nGO 3:1 at dry and wet state. The insets in both figures show the α of each material.

3.1.2. Microscopy and porosity characterization

SEM images of freeze dried and gold coated Chi:nGO 3:1 particles with increasing magnification are presented in Fig 3. The aim of the microscopic analysis is to describe both the topography of the material and an overview of the porous size distribution. Fig. 3a) shows the macroscopic appearance of the material after its sieving and the Fig. 3b) confirms the homogeneous particle size distribution with an average diameter around 200 µm. A closer view in the last two images indicates a highly heterogeneous distribution of the size and shape of pores; furthermore, in Fig. 3d) it can be appreciated the presence of sub-micrometric and nanometric pores within the cavity of larger pores. The MIP result supports this appreciation since it is found a wide pore size distribution with variable diameters ranging from 10 nm to 10 µm and multiple maxima (Supplementary data 2). In conclusion, this material cannot be classified according to its porosity.

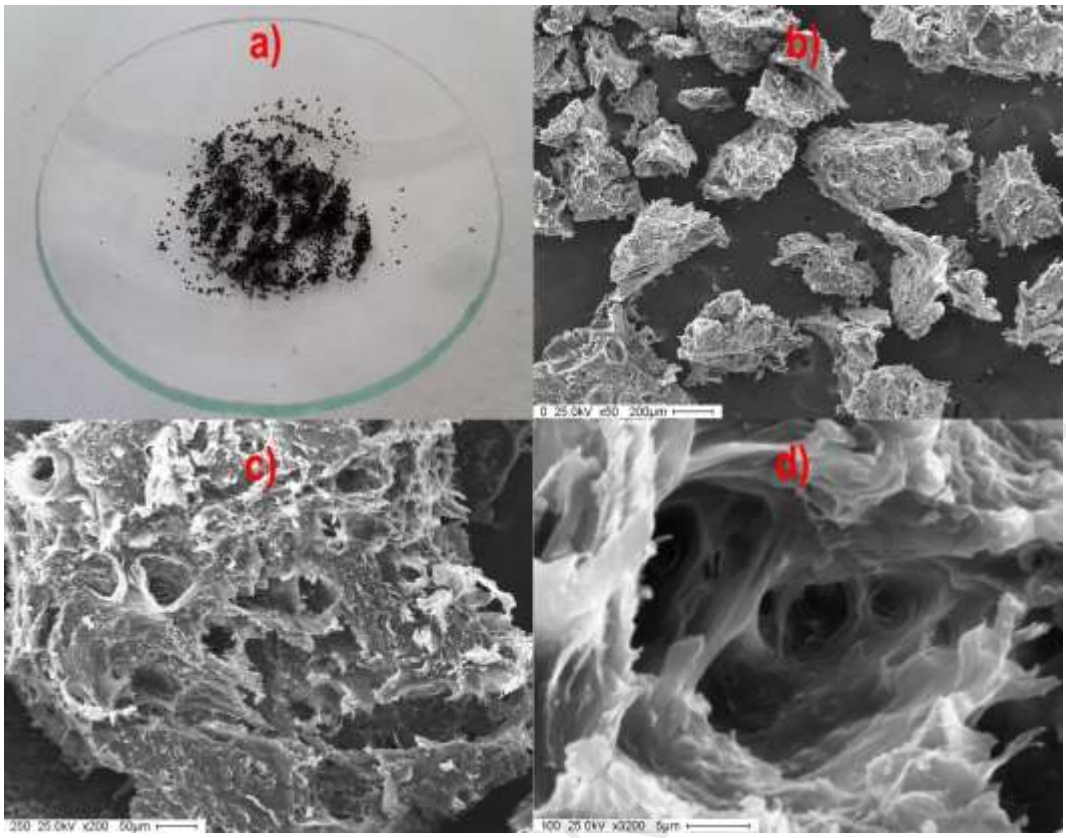

Fig. 3. Macroscopic and SEM images of Chi:nGO 3:1 with increasing magnification (b x50, c x200 and d x3200).

3.2. Adsorption isotherms

The equilibrium assays were carried out in ultra-pure water (pH ≈ 6.30) and all the absorbance measurements were done once the equilibrium was achieved and the results were expressed as q_e (mg/g), i.e. milligram of sorbate per gram of adsorbent, against ciprofloxacin concentration at equilibrium C_{eq} (mg/L). In order to obtain a better description of the adsorption process, all the results were analyzed through the non-linear form of three two-parameters isotherm models (Langmuir, Freundlich and Dubinin–Radushkevich) and two three-parameters models (Redlich–Peterson and Sips) (Altenor et al., 2009; Fu, Zhang, Lv, Chu, & Shang, 2012).

In Supplementary data 3 are presented all the assessed models with their non-linear equations and a Table that summarizes all the parameters and the RMSE. The Fig. 4 exhibits the isotherm adsorption curve which adjusted better to the Sips model. This model combines characteristics of Langmuir and Freundlich

depending on the concentration of sorbate. At low sorbate concentrations, it effectively reduces to a Freundlich isotherm and, thus, does not obey Henry's law. At high sorbate concentrations, it predicts a monolayer sorption capacity characteristic of the Langmuir isotherm (Foo & Hameed, 2010). Sips model has a heterogeneity parameter represented by n_s which, for this batch adsorption, is far from 1 (n_s = 0.38 ± 0.09) suggesting a heterogeneous sorption. This result would be explained based on the ciprofloxacin molecular structure which has three nitrogen atoms with basic properties and two unsaturated condensed and planar rings in its structure. Therefore, it could interact by both via electrostatic attraction and by π-π stacking with the acidic groups and unsaturated hexagonal rings of nGO, respectively (F. Wang et al., 2016). As can be appreciated, the adsorption capacity of Chi is one order of magnitude lower than that of Chi:nGO approximately, therefore all the subsequent assays were carried out using only the hybrid material. This difference in the adsorption capacity would be attributed to the lack of ionizable groups in the chitin structure in comparison with the hybrid and the multiple interaction sites present in the latter. Finally, in the case of pure nGO, the adsorption capacity exceeded the one of Chi:nGO 3:1 (q_m = 282 ± 11 mg/g vs 73 ± 3 mg/g respectively, modeled by the Langmuir model). As could be expected, the presence of chitin (with much less reactivity against ciprofloxacin) reduces the adsorption capacity of the composite since it presents a 25 % w/w of nGO.

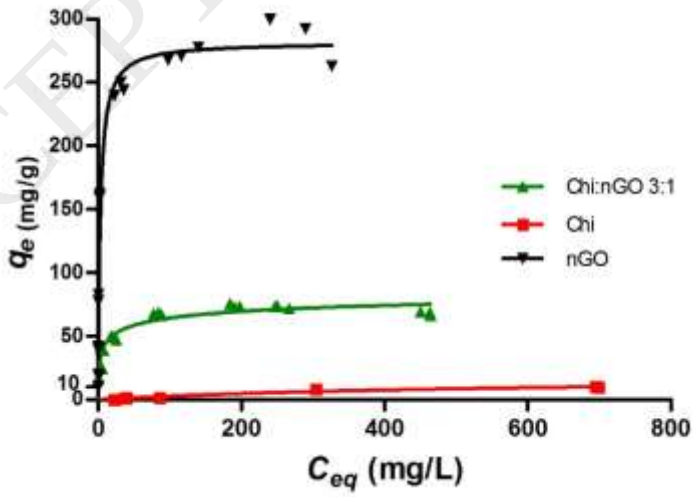

Fig. 4. Adsorption isotherms of ciprofloxacin using Chi:nGO 3:1, Chi and nGO. The best fitted model is plotted for each sample.

3.3. Column adsorption behavior

3.3.1. Effect of flow rate, pH, sodium and calcium presence

Fig. 5 exhibits all the breakthrough curves under the tested conditions. The Fig. 5a) shows the breakthrough curves at increasing flow rate (1 to 4 mL/min) at constant bed height and influent concentration. As can be seen, for higher flow rates the breakthrough times of the adsorption process become lower. The parameter τ from the Yoon-Nelson model (Table 1), which is the time required for 50 % adsorbate breakthrough, confirms this result since τ decreases as the flow rate increases. One interesting observation is that Thomas q_0 increases with flow rate. This phenomenon would be explained in terms of the adsorption mechanism on this kind of material which at low flow rates ciprofloxacin would interact mainly with the exposed surface and larger pores, and inner pores will be slowly filled. On the other hand, an increment in the flow represents higher availability of ciprofloxacin for the external sites that rapidly saturate and the remnant ciprofloxacin is forced to be adsorbed on the inner pores surface at lower kinetic rates, probably driven by an intrapellet diffusion mechanisms (Xu, Cai, & Pan, 2013). Considering SEM and MIP results mentioned in the characterization section, it could be expected that the ciprofloxacin adsorption mechanism would involve its interaction with all kind of existing pores and mainly with the external surface of the particle. The latter would be favored with respect to the inner pore surface at low flow rates or, at least, this phenomenon would be negligible.

It was demonstrated that the pH of the medium represents a very important parameter to consider for the continuous adsorption of ciprofloxacin on the hybrid material. Both acidic and basic pH (4.00 and 9.00) shift the breakthrough curve to lower times, especially at pH 9.00 where the C_t/C_0 ratio increases at very short times (Fig. 5b)). This behavior would be due by the distribution of ciprofloxacin species and the charge density of the nGO present in the material according to the medium pH. At pH 9.00, ciprofloxacin has a net negative charge due to its carboxylate group (pKa 3.01) and is strongly repealed from Chi:nGO 3:1 which has a pH_{pzc} near to 5.50 (Supplementary data 4) (Chen et al., 2015; Qiang & Adams, 2004). In the case of pH 4.00 the ciprofloxacin carboxyl group is negatively charged whereas its nitrogen atoms are predominantly protonated and

positively charged, however, this pH is below the material pH_{pzc}. Therefore, at this pH the main interactions between the sorbate and the hybrid would imply other kind of interactions instead of electrostatic attraction. There could be proposed the presence of hydrogen bondings with nGO oxidized functional groups and/or π-π stacking between the flat aromatic sections of nGO and the aromatic rings of ciprofloxacin. The n_s parameter of the Sips model in the isotherm analysis, which indicates a heterogeneous adsorption, and the dynamic capacity of the Thomas model (q_0) support this conclusion since the highest q_0 corresponds to the breakthrough curve at pH 4.00. When the electrostatic interaction is unfavored, the hydrophobic adsorption would take a very important role in the removal of ciprofloxacin.

Effects of the sodium concentration and the hardness of water are shown in Fig. 5c) and d). It is interesting that both cations produced different shifts in the breakthrough curves of ciprofloxacin adsorption. Firstly, Na^+ not only affects the curves shape but also increases the breakthrough times as the cation concentration raises as can be appreciated in the Yoon-Nelson τ parameter. Furthermore, the q_0 of Thomas model increases according to the Na^+ concentration. These results indicate that the salinity (i.e. concentration of sodium salts) would shield the electrostatic interaction between the matrix and ciprofloxacin and favors the hydrophobic interaction via a *salting out effect*. Secondly, the hardness of water (expressed as mg/L of $CaCO_3$) produced a similar effect to Na^+ in terms of dynamic capacity (q_0) and τ times. An increment in the Ca^{+2} concentration produces larger breakthrough times; however, as can be seen in the first section of the curves in Fig. 5d), Ca^{2+} rapidly increases the C_t/C_0 ratio due to the interaction of the divalent cation with nGO. Chowdhury *et al.* studied the behavior of nGO in different aquatic environments including salt types and concentration (Chowdhury, Duch, Mansukhani, Hersam, & Bouchard, 2013). They demonstrated that divalent cations (i.e. Ca^{2+} and Mg^{2+}) destabilizes nGO, specially Ca^{+2} due to the binding capacity of this ion with hydroxyl and carbonyl functional groups of nGO. In the Hofmeister series, which explains the interfacial phenomena according to the ionic composition of a certain medium, sodium is one of the earliest member of the series producing an increase in solvent surface tension and a decrease the solubility of non-polar molecules (*salting out effect*) (Cacace, Landau, & Ramsden, 1997). By contrast, near the end of the series is

located calcium which tends to increase the solubility of non-polar molecules and produces a chaotropic effect.

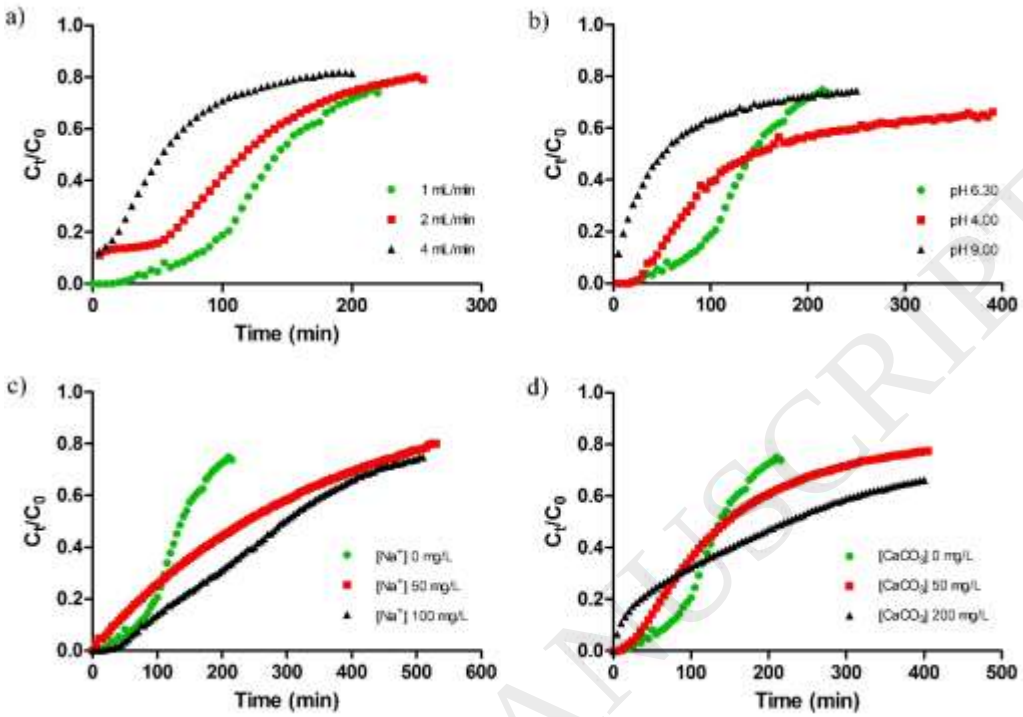

Fig. 5. Breakthrough curves for the different experimental conditions. Effect of flow rate (a), pH (b), Na^+ concentration (c) and water hardness as $CaCO_3$ (d).

3.3.2. Adsorption of ciprofloxacin in real water samples

Fig. 6 and Table 2 show the continuous adsorption performance of spiked ciprofloxacin from real water samples and the physicochemical profile with the breakthrough model parameters, respectively. Each real water cationic composition could be explained in terms of their different location sources. As can be observed, the complex matrix of real water interferes with the adsorption of ciprofloxacin on the material shifting the breakthrough curves to lower times especially in the cases of Chascomús and Macachín cities which have less than half of τ of ultra-pure water and Buenos Aires curves. Moreover, there is an important decrease in the q_0 of the first two cases. Is interesting that Buenos Aires's q_0 and τ parameters are not appreciable different in comparison with the spiked ultra-pure water breakthrough curve and the only difference is a decrease in the kinetic rate parameter k_{Th} of the Buenos Aires sample. Albeit the coexistence of cations influence was demonstrated, the overall behavior of the

breakthrough curves would be mainly lead by the medium pH since it establishes the kind of interaction.

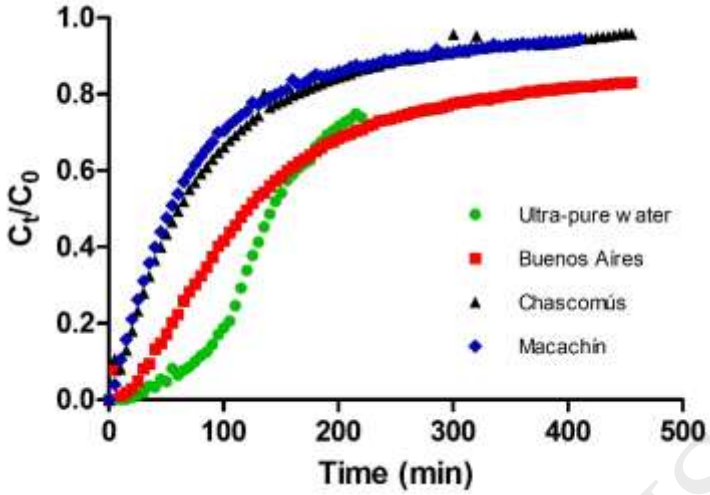

Fig 6. Breakthrough curves for the real water samples and ultra-pure water.

4. Conclusions

The Chi:nGO 3:1 hybrid material showed to be applicable for the removal of ciprofloxacin in a continuous system. Its high and wide size porosity endow to the material with a low flow resistance which allows to work at different flow rates. The isotherm assays demonstrated that the adsorption mechanism involves a heterogeneous process since it fitted better to the Sips model with a heterogeneity parameter far from the unit. The tested medium conditions and the real water samples experiments showed that the type of interaction, both electrostatic attraction or π-π stacking, and hence breakthrough times, are strongly dependent on the pH and the cation composition. Basing on this behavior we can predict the performance of the system in future applications taking into account the kind of sample that will be treated by the column adsorbent. Finally, this work contributes to the expansion of the applications of nanostructured materials that contain nGO within its composition since there is no evidence in literature of research articles that use this kind of materials in continuous systems.

Acknowledgments

J.A.G. is grateful for his doctoral fellowship granted by Consejo Nacional de Investigaciones Científicas y Técnicas (CONICET). M.E.V. is grateful for her postdoctoral fellowship granted by CONICET. The authors are grateful to the Brazilian Synchrotron Light Laboratory (LNLS) for SAXS facilities and would like to acknowledge INTI Mecánica for their assistance in SEM analysis. This work was supported with grants from Universidad de Buenos Aires (UBACYT 20020130100780BA) and Agencia Nacional de Promoción Científica y Tecnológica (PICT 2015-0714).

References

Altenor, S., Carene, B., Emmanuel, E., Lambert, J., Ehrhardt, J.-J., & Gaspard, S. (2009). Adsorption studies of methylene blue and phenol onto vetiver roots activated carbon prepared by chemical activation. *Journal of Hazardous Materials*, *165*(1–3), 1029–1039. https://doi.org/10.1016/j.jhazmat.2008.10.133

Beaucage, G. (1996). Small-Angle Scattering from Polymeric Mass Fractals of Arbitrary Mass-Fractal Dimension. *Journal of Applied Crystallography*, *29*(2), 134–146. https://doi.org/10.1107/S0021889895011605

Bonaccorso, F., Colombo, L., Yu, G., Stoller, M., Tozzini, V., Ferrari, A. C., … Pellegrini, V. (2015). Graphene, related two-dimensional crystals, and hybrid systems for energy conversion and storage. *Science*, *347*(6217), 1246501.

Breßler, I., Kohlbrecher, J., & Thünemann, A. F. (2015). *SASfit* : a tool for small-angle scattering data analysis using a library of analytical expressions. *Journal of Applied Crystallography*, *48*(5), 1587–1598. https://doi.org/10.1107/S1600576715016544

Brinker, C. J., Keefer, K. D., Schaefer, D. W., Assink, R. A., Kay, B. D., & Ashley, C. S. (1984). Sol-gel transition in simple silicates II. *Journal of Non-Crystalline Solids*, *63*(1–2), 45–59. https://doi.org/10.1016/0022-3093(84)90385-5

Brugnerotto, J., Lizardi, J., Goycoolea, F. ., Argüelles-Monal, W., Desbrières, J., & Rinaudo, M. (2001). An infrared investigation in relation with chitin and chitosan characterization. *Polymer*, *42*(8), 3569–3580. https://doi.org/10.1016/S0032-3861(00)00713-8

Cacace, M., Landau, E., & Ramsden, J. (1997). The Hofmeister series: salt and solvent effects on interfacial phenomena. *Quarterly Reviews of Biophysics*, *30*(03), 241–277. https://doi.org/10.1017/S0033583597003363

Chen, H., Gao, B., & Li, H. (2015). Removal of sulfamethoxazole and ciprofloxacin from aqueous solutions by graphene oxide. *Journal of Hazardous Materials*, *282*, 201–207. https://doi.org/10.1016/j.jhazmat.2014.03.063

Choudhary, S., & Bhatia, S. R. (2012). Rheology and nanostructure of hydrophobically modified alginate (HMA) gels and solutions. *Carbohydrate Polymers*, *87*(1), 524–530. https://doi.org/10.1016/j.carbpol.2011.08.025

Chowdhury, I., Duch, M. C., Mansukhani, N. D., Hersam, M. C., & Bouchard, D. (2013). Colloidal properties and stability of graphene oxide nanomaterials in the aquatic environment. *Environmental Science & Technology*, *47*(12), 6288–6296. https://doi.org/10.1021/es400483k

Fick, J., Söderström, H., Lindberg, R. H., Phan, C., Tysklind, M., & Larsson, D. G. J. (2009). CONTAMINATION OF SURFACE, GROUND, AND DRINKING WATER FROM PHARMACEUTICAL PRODUCTION.

Environmental Toxicology and Chemistry, *28*(12), 2522. https://doi.org/10.1897/09-073.1

Focher, B., Naggi, A., Torri, G., Cosani, A., & Terbojevich, M. (1992). Structural differences between chitin polymorphs and their precipitates from solutions—evidence from CP-MAS 13C-NMR, FT-IR and FT-Raman spectroscopy. *Carbohydrate Polymers*, *17*(2), 97–102. https://doi.org/10.1016/0144-8617(92)90101-U

Foo, K. Y., & Hameed, B. H. (2010). Insights into the modeling of adsorption isotherm systems. *Chemical Engineering Journal*, *156*(1), 2–10. https://doi.org/10.1016/j.cej.2009.09.013

Fu, D., Zhang, Y., Lv, F., Chu, P. K., & Shang, J. (2012). Removal of organic materials from TNT red water by Bamboo Charcoal adsorption. *Chemical Engineering Journal*, *193–194*, 39–49. https://doi.org/10.1016/j.cej.2012.03.039

Gonzalez, J. A., Mazzobre, M. F., Villanueva, M. E., Diaz, L. E., & Copello, G. J. (2014). Chitin hybrid materials reinforced with graphene oxide nanosheets: chemical and mechanical characterisation. *RSC Advances*, *4*(32), 16480–16488. https://doi.org/10.1039/C3RA47986B

González, J. A., Villanueva, M. E., Piehl, L. L., & Copello, G. J. (2015). Development of a chitin/graphene oxide hybrid composite for the removal of pollutant dyes: Adsorption and desorption study. *Chemical Engineering Journal*, *280*, 41–48. https://doi.org/10.1016/j.cej.2015.05.112

Guo, Y., Duan, B., Cui, L., & Zhu, P. (2015). Construction of chitin/graphene oxide hybrid hydrogels. *Cellulose*, *22*(3), 2035–2043. https://doi.org/10.1007/s10570-015-0630-2

Guo, Y., Duan, B., Zhou, J., & Zhu, P. (2014). Chitin/graphene oxide composite films with enhanced mechanical properties prepared in NaOH/urea aqueous solution. *Cellulose*, *21*(3).

Hadi, M., Samarghandi, M. R., & McKay, G. (2010). Equilibrium two-parameter isotherms of acid dyes sorption by activated carbons: Study of residual errors. *Chemical Engineering Journal*, *160*(2), 408–416. https://doi.org/10.1016/j.cej.2010.03.016

Han, R., Wang, Y., Zhao, X., Wang, Y., Xie, F., Cheng, J., & Tang, M. (2009). Adsorption of methylene blue by phoenix tree leaf powder in a fixed-bed column: experiments and prediction of breakthrough curves. *Desalination*, *245*(1–3), 284–297. https://doi.org/10.1016/j.desal.2008.07.013

Holmström, K., Gräslund, S., Wahlström, A., Poungshompoo, S., Bengtsson, B., & Kautsky, N. (2003). Antibiotic use in shrimp farming and implications for environmental impacts and human health. *International Journal of Food Science & Technology*, *38*(3), 255–266. https://doi.org/10.1046/j.1365-2621.2003.00671.x

Huang, Y., Fulton, A. N., & Keller, A. A. (2016). Optimization of porous structure of superparamagnetic nanoparticle adsorbents for higher and faster removal of emerging organic contaminants and PAHs. *Environ. Sci.: Water Res. Technol.*, *2*(3), 521–528. https://doi.org/10.1039/C6EW00066E

Hummers Jr, W. S., & Offeman, R. E. (1958). Preparation of graphitic oxide. *Journal of the American Chemical Society*, *80*(6), 1339–1339. https://doi.org/10.1021/ja01539a017

Ji, Y., Ferronato, C., Salvador, A., Yang, X., & Chovelon, J.-M. (2014). Degradation of ciprofloxacin and sulfamethoxazole by ferrous-activated persulfate: Implications for remediation of groundwater contaminated by

antibiotics. *Science of The Total Environment*, *472*, 800–808. https://doi.org/10.1016/j.scitotenv.2013.11.008

Li, R., Liu, C., & Ma, J. (2011). Studies on the properties of graphene oxide-reinforced starch biocomposites. *Carbohydrate Polymers*, *84*(1), 631–637. https://doi.org/10.1016/j.carbpol.2010.12.041

Lopez-Ramon, M. V., Stoeckli, F., Moreno-Castilla, C., & Carrasco-Marin, F. (1999). On the characterization of acidic and basic surface sites on carbons by various techniques. *Carbon*, *37*(8), 1215–1221. https://doi.org/10.1016/S0008-6223(98)00317-0

Ma, Z., Liu, D., Zhu, Y., Li, Z., Li, Z., Tian, H., & Liu, H. (2016). Graphene oxide/chitin nanofibril composite foams as column adsorbents for aqueous pollutants. *Carbohydrate Polymers*, *144*, 230–237. https://doi.org/10.1016/j.carbpol.2016.02.057

Matamoros, V., Rodríguez, Y., & Albaigés, J. (2016). A comparative assessment of intensive and extensive wastewater treatment technologies for removing emerging contaminants in small communities. *Water Research*, *88*, 777–785. https://doi.org/10.1016/j.watres.2015.10.058

McConville, P., Whittaker, M. K., & Pope, J. M. (2002). Water and Polymer Mobility in Hydrogel Biomaterials Quantified by ^{1}H NMR: A Simple Model Describing Both T_1 and T_2 Relaxation. *Macromolecules*, *35*(18), 6961–6969. https://doi.org/10.1021/ma020539c

McKay, G., Blair, H. S., & Gardner, J. R. (1984). The adsorption of dyes onto chitin in fixed bed columns and batch adsorbers. *Journal of Applied Polymer Science*, *29*(5), 1499–1514. https://doi.org/10.1002/app.1984.070290504

Ncibi, M. C., & Sillanpää, M. (2015). Optimized removal of antibiotic drugs from aqueous solutions using single, double and multi-walled carbon nanotubes. *Journal of Hazardous Materials*, *298*, 102–110. https://doi.org/10.1016/j.jhazmat.2015.05.025

Novoselov, K. S. (2004). Electric Field Effect in Atomically Thin Carbon Films. *Science*, *306*(5696), 666–669. https://doi.org/10.1126/science.1102896

Petrie, B., Barden, R., & Kasprzyk-Hordern, B. (2015). A review on emerging contaminants in wastewaters and the environment: Current knowledge, understudied areas and recommendations for future monitoring. *Occurrence, Fate, Removal and Assessment of Emerging Contaminants in Water in the Water Cycle (from Wastewater to Drinking Water)*, *72*, 3–27. https://doi.org/10.1016/j.watres.2014.08.053

Prieto, A., Möder, M., Rodil, R., Adrian, L., & Marco-Urrea, E. (2011). Degradation of the antibiotics norfloxacin and ciprofloxacin by a white-rot fungus and identification of degradation products. *Bioresource Technology*, *102*(23), 10987–10995. https://doi.org/10.1016/j.biortech.2011.08.055

Qiang, Z., & Adams, C. (2004). Potentiometric determination of acid dissociation constants (pKa) for human and veterinary antibiotics. *Water Research*, *38*(12), 2874–2890. https://doi.org/10.1016/j.watres.2004.03.017

Rodriguez-Narvaez, O. M., Peralta-Hernandez, J. M., Goonetilleke, A., & Bandala, E. R. (2017). Treatment technologies for emerging contaminants in water: A review. *Chemical Engineering Journal*, *323*, 361–380. https://doi.org/10.1016/j.cej.2017.04.106

Saito, Y., Putaux, J., Okano, T., Gaill, F., & Chanzy, H. (1997). Structural aspects of the swelling of β chitin in HCl and its conversion into α chitin. *Macromolecules*, *30*(13), 3867–3873. https://doi.org/10.1021/ma961787+

Sharif, F., Gagnon, L. R., Mulmi, S., & Roberts, E. P. L. (2017). Electrochemical regeneration of a reduced graphene oxide/magnetite composite adsorbent loaded with methylene blue. *Water Research*, *114*, 237–245. https://doi.org/10.1016/j.watres.2017.02.042

Sharma, V. K., Johnson, N., Cizmas, L., McDonald, T. J., & Kim, H. (2016). A review of the influence of treatment strategies on antibiotic resistant bacteria and antibiotic resistance genes. *Chemosphere*, *150*, 702–714. https://doi.org/10.1016/j.chemosphere.2015.12.084

Suárez-Iglesias, O., Collado, S., Oulego, P., & Díaz, M. (2017). Graphene-family nanomaterials in wastewater treatment plants. *Chemical Engineering Journal*, *313*, 121–135. https://doi.org/10.1016/j.cej.2016.12.022

Tamura, H., Nagahama, H., & Tokura, S. (2006). Preparation of chitin hydrogel under mild conditions. *Cellulose*, *13*(4), 357–364. https://doi.org/10.1007/s10570-006-9058-z

Teuber, M. (2001). Veterinary use and antibiotic resistance. *Current Opinion in Microbiology*, *4*(5), 493–499. https://doi.org/10.1016/S1369-5274(00)00241-1

Van Doorslaer, X., Dewulf, J., Van Langenhove, H., & Demeestere, K. (2014). Fluoroquinolone antibiotics: an emerging class of environmental micropollutants. *Science of the Total Environment*, *500*, 250–269. https://doi.org/10.1016/j.scitotenv.2014.08.075

Wang, F., Yang, B., Wang, H., Song, Q., Tan, F., & Cao, Y. (2016). Removal of ciprofloxacin from aqueous solution by a magnetic chitosan grafted

graphene oxide composite. *Journal of Molecular Liquids*, *222*, 188–194. https://doi.org/10.1016/j.molliq.2016.07.037

Wang, Y., Shen, C., Zhang, M., Zhang, B.-T., & Yu, Y.-G. (2016). The electrochemical degradation of ciprofloxacin using a SnO2-Sb/Ti anode: Influencing factors, reaction pathways and energy demand. *Chemical Engineering Journal*, *296*, 79–89. https://doi.org/10.1016/j.cej.2016.03.093

Xu, Z., Cai, J., & Pan, B. (2013). Mathematically modeling fixed-bed adsorption in aqueous systems. *Journal of Zhejiang University SCIENCE A*, *14*(3), 155–176. https://doi.org/10.1631/jzus.A1300029

Yan, Y., Sun, S., Song, Y., Yan, X., Guan, W., Liu, X., & Shi, W. (2013). Microwave-assisted in situ synthesis of reduced graphene oxide-BiVO4 composite photocatalysts and their enhanced photocatalytic performance for the degradation of ciprofloxacin. *Journal of Hazardous Materials*, *250–251*, 106–114. https://doi.org/10.1016/j.jhazmat.2013.01.051

Zhang, Q., Shan, G., Cao, P., He, J., Lin, Z., Huang, Y., & Ao, N. (2015). Mechanical and biological properties of oxidized horn keratin. *Materials Science and Engineering: C*, *47*, 123–134. https://doi.org/10.1016/j.msec.2014.11.051

Table 1. Thomas and Yoon-Nelson parameter values for the different experimental conditions.

Condition		Flow rate (mL/min)	pH	Model					
				Thomas			Yoon-Nelson		
				q_0 (mg/g)	k_{Th} (mL/mg min)	RMSE	k_{YN} (min^{-1})	τ (min)	RMSE
Flow rate variation		1	6.30	53±1	0.69±0.05	0.1050	0.024±0.002	153±3	0.1050
		2	6.30	90±1	0.46±0.01	0.0537	(160±4)x10^{-4}	128±1	0.0537
		4	6.30	91±4	0.51±0.03	0.0770	0.018±0.001	65±3	0.0770
pH variation		1	4.00	72±3	0.19±0.01	0.0969	(67±5)x10^{-4}	207±7	0.1061
		1	9.00	24±2	0.25±0.02	0.0705	(86±7)x10^{-4}	69±6	0.0969
Na^+ (mg/L)	50	1	6.30	92±1	0.185±0.004	0.0569	(65±1)x10^{-4}	263±3	0.0569
	100	1	6.30	110±1	0.223±0.005	0.0524	(78±2)x10^{-4}	315±2	0.0524
$CaCO_3$ (mg/L)	50	1	6.30	64±1	0.257±0.008	0.0882	(90±3)x10^{-4}	182±3	0.0882
	200	1	6.30	84±1	0.167±0.004	0.0445	(58±1)x10^{-4}	241±3	0.0449

Table 2. Physicochemical characterization and breakthrough model parameters of real water samples.

Origin	pH	K^+ (mg/L)	Na^+ (mg/L)	Ca^{2+} (mg/L)	Mg^{2+} (mg/L)	$CaCO_3$ (mg/L)*	Model	
							Thomas	Yoon-Nelson

							q_0 (mg/g)	k_{Th} (mL/mg min)	RMSE	k_{YN} (min^{-1})	τ (min)	RMSE
Buenos Aires	7.99	7±2	34.8±0.8	17±1	1.8±0.1	49±4	54±2	0.27±0.01	0.1094	$(94\pm5)x10^{-4}$	154±5	0.1094
Chascomús	8.58	39±3	603±16	40±1	18.0±0.6	174±6	26.4±0.8	0.46±0.02	0.0644	$(160\pm6)x10^{-4}$	76±2	0.0644
Macachín	8.50	13±2	267±10	47±1	27.8±0.5	231±4	23.6±0.7	0.49±0.02	0.0734	$(58\pm1)x10^{-4}$	67±2	0.0734

*The hardness of water was calculated from the contribution of Ca^{2+} and Mg^{2+}.